Molecular Genetics and Metabolism Reports 10 (2017) 67–74

Contents lists available at ScienceDirect

Molecular Genetics and Metabolism Reports

journal homepage: www.elsevier.com/locate/ymgmr

Gene therapy for a mouse model of glucose transporter-1 deficiency syndrome

Sachie Nakamura [a], Hitoshi Osaka [a,*], Shin-ichi Muramatsu [b,g], Naomi Takino [b], Mika Ito [b], Shiho Aoki [a], Eriko F. Jimbo [a], Kuniko Shimazaki [c], Tatsushi Onaka [d], Sumio Ohtsuki [e], Tetsuya Terasaki [f], Takanori Yamagata [a]

[a] Department of Pediatrics, Jichi Medical University, Tochigi, Japan
[b] Division of Neurology, Jichi Medical University, Tochigi, Japan
[c] Department of Neurosurgery, Jichi Medical University, Tochigi, Japan
[d] Division of Brain and Neurophysiology, Department of Physiology, Jichi Medical University, Tochigi, Japan
[e] Department of Pharmaceutical Microbiology, Faculty of Life Sciences, Kumamoto University, Kumamoto, Japan
[f] Division of Membrane Transport and Drug Targeting, Graduate School of Pharmaceutical Sciences, Tohoku University, Sendai, Japan
[g] Center for Gene and Cell Therapy, The Institute of Medical Science, The University of Tokyo, Japan

ARTICLE INFO

Article history:
Received 18 October 2016
Accepted 30 December 2016
Available online 15 January 2017

Keywords:
Glucose transporter I deficiency syndrome (GLUT1DS)
GLUT1
SLC2A1
Adeno-associated virus (AAV)
Gene therapy

ABSTRACT

Objective: We generated an adeno-associated virus (AAV) vector in which the human *SLC2A1* gene was expressed under the synapsin I promoter (AAV-h*SLC2A1*) and examined if AAV-h*SLC2A1* administration can lead to functional improvement in *GLUT1*-deficient mice.
Methods: AAV-h*SLC2A1* was injected into heterozygous knock-out murine *Glut1* (GLUT1$^{+/-}$) mice intraperitoneally (systemic; 1.85×10^{11} vg/mouse) or intra-cerebroventricularly (local; 1.85×10^{10} vg/mouse). We analyzed GLUT1 mRNA and protein expression, motor function using rota-rod and footprint tests, and blood and cerebrospinal fluid (CSF) glucose levels.
Results: Vector-derived RNA was detected in the cerebrum for both injection routes. In the intracerebroventricular injection group, exogenous GLUT1 protein was strongly expressed in the cerebral cortex and hippocampus near the injection site. In the intraperitoneal injection group, exogenous GLUT1 protein was mildly expressed in neural cells throughout the entire central nervous system. The motor function test and CSF/blood glucose ratio were significantly improved following intra-cerebroventricular injection.
Conclusions: AAV-h*SLC2A1* administration produced exogenous GLUT1 in neural cells and improved CSF glucose levels and motor function of heterozygous knock-out murine Glut1 mice.

1. Introduction

Glucose transporter 1 deficiency syndrome (GLUT1DS; OMIM #606777) is an autosomal dominant disorder caused by haploinsufficiency of *SLC2A1*, the gene encoding GLUT1. GLUT1 is expressed in the central nervous system (CNS), mainly in the endothelial cells of the blood-brain barrier, but also in other types of cells including neurons [1–4]. GLUT1 interacts with other glucose transporters and mediates glucose transport into neurons [2,3,5]. Heterozygous mutation of *SLC2A1* leads to impaired hexose transport into the brain, resulting in irreversible neurologic dysfunction [6–8]. The biochemical hallmark for GLUT1DS is hypoglycorrhachia: cerebrospinal fluid (CSF) glucose level < 40 mg/dL and CSF/blood glucose ratio < 0.45 [8,9].

The classical symptoms of GLUT1DS are intractable seizures, intellectual disability, ataxia, and dystonia starting at infancy. In adulthood, some GLUT1DS patients develop paroxysmal exercise-induced dyskinesia [10]. The current and major therapy for GLUT1DS is a ketogenic diet, which is a high-fat, carbohydrate-restricted diet [11,12]. A ketogenic diet is effective for seizures, transient aggravation after fasting, and ataxia [12]. In addition, a modified Atkins diet may be effective for seizures and partially effective for cognitive function [13]. However, a ketogenic diet is not effective for the intellectual disability and movement disorder observed in adult patients with GLUT1DS [7,10,12] and can lead to hyperlipidemia and is considered a primary risk factor for the development of atherosclerosis [14]. The other treatment for GLUT1DS, triheptanoin, which is a medium chain triglyceride with odd chain fatty acids, has the potential to improve the paroxysmal motor disorder [15], but its long-term efficacy is unknown.

Recently, gene therapy has given remarkable results in various clinical trials and mouse models [16,17]. With its low immunogenicity and long-term expression in non-dividing post-mitotic neuronal cells, the

* Corresponding author at: Dept. of Pediatrics, Jichi Medical School, 3311-1 Yakushiji, Shimotsuke-shi, Tochigi 329-0498, Japan.
E-mail address: hosaka@jichi.ac.jp (H. Osaka).

http://dx.doi.org/10.1016/j.ymgmr.2016.12.008

adeno-associated viral vector (AAV) appears to be an optimal vehicle for the treatment of congenital CNS disorders [17]. Therefore, we aimed to develop gene therapy for GLUT1DS. To this end, we investigated if *SLC2A1* gene delivery using an AAV vector can lead to functional improvement in *GLUT1* - heterozygous knock-out murine mice.

2. Materials and methods

2.1. Glut1-deficient mice

Mice with heterozygous knock-out of the murine *Glut1* gene (GLUT1$^{+/-}$ mice) were generated by the Department of Molecular Biopharmacy and Genetics, Graduate School of Pharmaceutical Sciences, Tohoku University, Sendai, Japan [18]. The gene mutation of GLUT1$^{+/-}$ mice was created by the insertion of a gene-trapping vector that contains a splice acceptor site followed by a neomycin resistance (neo) gene with a polyadenylation signal in intron 1 of the *Glut1* gene. GLUT1$^{+/-}$ mice have microcephaly, impaired motor activity, epileptic discharges on electroencephalography, hypoglycorrhachia, and decreased brain glucose uptake by positron emission tomography scanning [18,19]. GLUT1$^{+/-}$ mice mimic the classical phenotype of human patients with GLUT1DS, and GLUT1$^{-/-}$ mice were embryonic lethal. All animal studies were approved by the Animal Care Committee, Jichi Medical University (approval number, 16-192).

2.2. Generation of AAV vectors

The AAV vector plasmids contained an expression cassette consisting of the neuron-specific synapsin I promoter, followed by human *SLC2A1*, sharing high homology with mouse GLUT1 (96% identical at the amino acid level) with or without myc-DDK (FLAG®), and a simian virus 40 polyadenylation signal sequence between the inverted terminal repeats of the AAV3 genome (Fig. 1). We synthesized the AAV9 *vp* cDNA as described previously [20] with the substitution of thymidine for adenine 1337, which introduced an amino acid change from tyrosine to phenylalanine at position 446. Recombinant AAV vectors were produced by transient transfection into HEK293 cells using the vector plasmid, an AAV3 *rep* and AAV9 *vp* expression plasmid, and the adenoviral helper plasmid pHelper (Agilent Technologies, Santa Clara, CA). We purified the recombinant viruses by isolation from two sequential continuous CsCl gradients, and viral titers were determined by quantitative PCR.

2.3. Infection of neuronal SH-SY5Y cells with AAV-hSLC2A1

The human neuroblastoma SH-SY5Y cell line was seeded in an 8-well chamber slide (0.8 cm^2/well at 1.0×10^5 cells/well). After an overnight incubation at 37 °C, the cells were infected with AAV-h*SLC2A1* at 3.7×10^9 vg/well. At 40 h after infection with AAV-h*SLC2A1*, the SH-SY5Y cells were fixed with 4% paraformaldehyde for 15 min. After 3 washes with phosphate-buffered saline (PBS) for 5 min, the fixed cells were incubated with blocking buffer (PBS containing 4% goat serum, 0.1% Triton X-100) for 1 h at room temperature (RT) and incubated with primary antibodies (containing blocking buffer) overnight at 4 °C. The following primary antibodies were used: mouse monoclonal anti-c-myc (9E10) (sc-40; Santa Cruz Biotechnology, Santa Cruz, CA) at 1:150 and rabbit polyclonal anti-GLUT1 (N-terminus) (TA301678; OriGene Technologies, Rockville, MD) at 1:100. After 3 washes with 0.1% Triton X-100, immune-complexes were detected using the following secondary antibodies (for 2 h at RT): goat anti-mouse IgG Alexa Fluor 594 (Invitrogen, Carlsbad, CA) at 1:250 and goat anti-rabbit IgG Alexa Fluor 488 (Invitrogen, Carlsbad, CA) at 1:250. Hoechst 33342 was used to visualize nuclei. Confocal images were acquired with a FluoView™ FV1000 confocal microscope (Olympus, Tokyo, Japan).

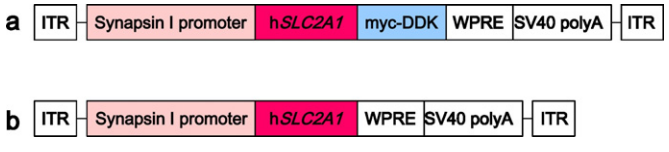

Fig. 1. Structure of AAV-h*SLC2A1*. We selected the neuron-specific synapsin I promoter for the expression of *SLC2A1* in neural cells with a reduced off-target effect [20,24,25]. The human *SLC2A1* sequence was fused with a myc-DDK (FLAG®) tag at its C-terminus (a). We also created a tag sequence-removed AAV-h*SLC2A1* to assess its clinical application (b). ITR: inverted terminal repeat; WPRE: woodchuck hepatitis virus posttranscriptional regulatory element; SV40 polyA: simian virus 40 poly A.

2.4. Systemic or intra-cerebroventricular injection of GLUT1$^{+/-}$ mice with AAV-hSLC2A1

For systemic administration, AAV-h*SLC2A1* (1.85×10^{11} vg; total 50 μL/mouse) was injected into the peritoneum at 7 days after birth, because brain tissue was less damaged at the early neonatal period. For CNS administration, AAV-h*SLC2A1* (1.85×10^{10} vg; total 5 μL/mouse) was injected directly into the bilateral lateral ventricles of the brain at 6 weeks after birth, because patients with GLUT1DS are diagnosed from the infant to childhood period [6–8]. We could not observe any symptoms for GLUT1$^{+/-}$ mice at 6 weeks. Intra-cerebroventricular injections of GLUT1$^{+/-}$ mice were performed using a sharp glass electrode under intraperitoneal 2% chloral hydrate anesthesia. The injection site was measured relative to the bregma: 0.5 mm posterior to the bregma, 1.0 mm laterally from the sagittal suture, and 1.75 mm depth. For control GLUT1$^{+/-}$ mice, saline (total 5 μL) was injected into the bilateral lateral ventricles of the brain at 6 weeks after birth.

2.5. Analysis of exogenous and endogenous GLUT1 mRNA expression by reverse transcriptase-polymerase chain reaction (RT-PCR)

2 months after AAV-h*SLC2A1* injection, mice were sacrificed under CO_2 anesthesia. Total RNA was extracted from the whole cerebrum of mice using the TRIzol® reagent (Invitrogen, Carlsbad, CA). We reverse transcribed 2.5 μg total RNA to cDNA using a SuperScript® VILO™ cDNA Synthesis Kit (Invitrogen, Carlsbad, CA), followed by PCR amplification using TaKaRa Taq™ DNA Polymerase (TAKARA BIO, INC., Otsu, Japan). To confirm the expression of exogenous *GLUT1* mRNA, a reverse primer for vector specific RT-PCR was designed according to the myc-tag sequence: forward primer 5′-ACTGTCGTGTCGCTGTTTG-3′, reverse primer 5′-TGCTGCCAGATCCTCTTCTG-3′. PCR was conducted with the following cycling conditions: 1 cycle at 94 °C for 3 min, 27 cycles at 94 °C for 30 s, 58 °C for 30 s, and 72 °C for 30 s, and a final elongation step at 72 °C for 10 min. Additionally, we confirmed the total amount of *GLUT1* mRNA expression using primers corresponding to both the human *SLC2A1* and murine *Slc2a1* sequences: forward primer 5′-AACTGGGCAAGTCCTTTG-3′, reverse primer 5′-TTCTTCTCCCGCATCATCTG-3′. PCR was conducted with the following cycling conditions: 1 cycle at 94 °C for 3 min, 25 cycles at 94 °C for 30 s, 54 °C for 30 s, and 72 °C for 30 s, and a final elongation step at 72 °C for 10 min. Primers were designed for glyceraldehyde 3-phosphate dehydrogenase (*G3PDH*) mRNA as a quantitative control: forward primer 5′-ACCACAGTCCATGCCATCAC-3′, reverse primer 5′-TCCACCACCCTGTTGCTGTA-3′ (TOYOBO, Osaka, Japan). PCR was conducted with the following cycling conditions: 1 cycle at 94 °C for 3 min, 25 cycles at 94 °C for 30 s, 58 °C for 30 s, and 72 °C for 30 s, and a final elongation step at 72 °C for 10 min.

2.6. Quantitative real-time PCR analysis

Single-strand cDNA was synthesized from 2.5 μg total RNA by reverse transcription. According to the manufacturer's protocol, quantitative real-time PCR was performed using an Applied Biosystems® 7500 Fast Real-Time PCR System (Applied Biosystems, Life Technologies, Carlsbad, CA) with 2× TaqMan® Fast Universal PCR Master Mix, reverse transcribed cDNA, primers, and fluorescently-labeled probes. To confirm the

expression of exogenous *GLUT1* mRNA, a reverse primer was designed according to the myc-tag sequence: forward primer 5′-TTCGATGAGATCGCTTCCG-3′, reverse primer 5′-CTCTTCTGAGATGAGTTTCTGC-3′. The sequence of the dual fluorescently-labeled (FAM/TAMRA) probe was: 5′-TGGAACAGCTCCTCGGGTGTCTTGTCACTTTG-3′. We confirmed the total amount of *GLUT1* mRNA expression using primers corresponding to human *SLC2A1* and murine *Slc2a1* sequences: forward primer 5′-AAGTCCTTTGAGATGCTGATCC-3′, reverse primer 5′-CCCACATACATG GGCAC-3′. The sequence of the dual fluorescently-labeled (FAM/TAMRA) probe was: 5′-TCAGGCCGCAGTACACACCGATGATGAA-3′. The endogenous control assay was murine *Gapdh* by TaqMan® Gene Expression Assays (Mm00484668_m1; Applied Biosystems, Life Technologies, Carlsbad, CA). PCR was conducted with the following cycling conditions: 1 cycle at 95 °C for 20 s, and 40 cycles at 95 °C for 3 s and 60 °C for 30 s.

2.7. Brain tissue preparation and immunofluorescence assay

The brain was eviscerated and fixed with 4% paraformaldehyde overnight at 4 °C. Following fixation, the brain was transferred to 10–30% sucrose with PBS in stages and embedded in Tissue-Tek® O.C.T.™ Compound (Sakura Finetek Japan, Tokyo, Japan). Sagittal cryostat sections of 10 μm were collected on 3-aminopropyl triethoxy silane-coated glass slides and stored at − 80 °C. Tissue sections were washed 3 times with PBS for 5 min. After washing, the tissue sections were rinsed with blocking buffer (PBS containing 4% goat serum, 0.1% Triton X-100) for 30 min at RT and incubated with a primary antibody (containing blocking buffer) overnight at 4 °C. The following primary antibodies were used: rabbit polyclonal anti-myc-tag (562; MBL, Nagoya, Japan) at 1:250 and rabbit polyclonal anti-GLUT1 (N-terminus) (TA301678; OriGene Technologies, Rockville, MD) at 1:100. After 3 washes with 0.1% Triton X-100, immune-complexes were detected using the following secondary antibody (1 h at 37 °C): goat anti-rabbit IgG Alexa Fluor 488 (Invitrogen, Carlsbad, CA) at 1:250. Hoechst 33342 was used to visualize nuclei. Fluorescence staining was observed using an upright fluorescence microscope (AX70; Olympus, Tokyo, Japan). Next, we examined the derivation of myc-immunoreactive cells. Brain tissue sections were stained using an anti-myc-tag antibody and the following primary antibodies: chicken polyclonal anti-beta III tubulin (ab107216; Abcam Plc., Cambridge, UK) at 1:3000, goat polyclonal anti-PLP1 (sc-18529; Santa Cruz Biotechnology, Santa Cruz, CA) at 1:50, goat polyclonal anti-GFAP (sc-6170; Santa Cruz Biotechnology, Santa Cruz, CA) at 1:50, and goat polyclonal anti-CD31/PECAM-1 (AF3628; R&D Systems, Inc., Minneapolis, MN) at 1:45. Immunocomplexes were detected using the following secondary antibodies: donkey anti-rabbit IgG Alexa Fluor 488, donkey anti-goat IgG Alexa Fluor 594, and goat anti-chicken IgY Alexa Fluor 594 (Invitrogen, Carlsbad, CA) at 1:250.

2.8. Western blot analysis

2 months after AAV-h*SLC2A1* injection, mice were sacrificed under CO_2 anesthesia and the forebrain was eviscerated. Brain protein was extracted in a homogenization buffer (50 mM NaF, 5 mM EDTA [pH 7.4], 1% Triton X-100 dissolved in PBS) with 1 protease inhibitor tablet (Sigma*FAST*™; Sigma-Aldrich, St. Louis, MO) and 1 mM PMSF (Sigma), and sonicated. Following sonication, all samples were incubated on ice for 30 min, then centrifuged at 20,600 × *g* for 30 min at 4 °C. The supernatant was transferred to a fresh tube. Protein concentration was determined using a Qubit® Protein Assay Kit (Invitrogen, Carlsbad, CA). The supernatant was mixed with an equal volume of 2× sodium dodecyl sulfate (SDS) sample buffer and boiled. Western blots were performed using 10 μg total protein. Protein samples were resolved by 10% SDS-polyacrylamide gel electrophoresis (PAGE) followed by electro-transfer of the proteins onto a polyvinylidene fluoride (PVDF) membrane. The membrane was blocked for 1 h at RT using 5% skimmed milk/PBS with Tween® (PBST), then incubated with the following primary antibodies: rabbit polyclonal anti-GLUT1 (N-terminus) (TA301678; OriGene Technologies, Rockville, MD) at 1:500 and mouse monoclonal anti-beta-actin (A1978; Sigma-Aldrich, St. Louis, MO) at 1:2000 in PBST overnight at 4 °C. After washing with PBST 3 times for 10 min, the membrane was incubated the following secondary antibodies: anti-rabbit IgG horse radish peroxidase (HRP) (Santa Cruz Biotechnology, Santa Cruz, CA) at 1:2000 and anti-mouse IgG HRP (Santa Cruz Biotechnology, Santa Cruz, CA) at 1:2000 for 1 h at RT. After washing with PBST 3 times for 15 min, the membrane was incubated with HRP Substrate (TAKARA BIO, INC., Otsu, Japan) for 2 min. Finally, chemiluminescence from the membrane was imaged using ImageQuant LAS 4000 (GE Healthcare UK Ltd., Little Chalfont, UK).

2.9. Rota-rod test

Mice (at 10 and 14 weeks old; corresponding to 4 and 8 weeks after intra-cerebroventricular injection, respectively) were placed on a single-lane rotating drum (3 cm diameter) (O′Hara and Co., Tokyo, Japan and Muromachi Kikai Co., Ltd., Tokyo, Japan). The speed of the Rota-rod increased from 4 to 40 rotations over a 5-min period. The mice were trained by being placed individually on the rotating drum in acceleration mode from 4 to 40 rpm 3 times daily for 2 continuous days. On the second day, at 30 min after the final training session, the mice were tested in acceleration mode from 4 to 40 rpm. The time taken to fall off the rotating drum was recorded.

2.10. Footprint test

Mice (10 and 14 weeks old; corresponding to 4 and 8 weeks after intra-cerebroventricular injection, respectively) were trained 2 times daily for 2 continuous days to walk along a 50-cm-long, 10-cm-wide corridor (with 30-cm-high walls) toward a dark compartment. Before the trial, a sheet of white paper was put on the floor of the runway and their hind paws were dipped in India ink and were then allowed to walk on paper strips. Stride length and interstep and hindpaw base width were measured from 3 steps; the mean value of each set of 3 steps was used in the analysis.

2.11. Blood glucose and CSF glucose measurements

Blood glucose and CSF glucose measurements were performed using 14-week-old mice; corresponding to 8 weeks after intra-cerebroventricular injection. The mice were fasted overnight and anesthetized by intraperitoneal injection of 2% chloral hydrate. Blood was obtained from the tail vein, and blood glucose was measured by ACCU CHECK Aviva (Roche Diagnostics K.K., Tokyo, Japan). CSF was isolated from the cisterna magna as described previously with modifications [21] and measured using a FUJI DRI-CHEM 3500V Chemistry Analyzer (FUJIFILM Holdings Corporation, Tokyo, Japan).

2.12. Statistical analysis

Data are expressed as the mean ± standard error of the mean. Student's *t*-test was used for comparisons between two groups, and Dunnett's test was used for multiple comparisons. The significance level for statistical comparison was $P < 0.05$.

3. Results

3.1. Preparation of AAV-hSLC2A1 and Glut1-deficient mice

We generated AAV vectors expressing human *SLC2A1* tagged with or without myc-DDK (FLAG®) (AAV-h*SLC2A1*). The AAV vectors consisted of the tyrosine mutant AAV9 capsid and can cross the blood-brain

barrier efficiently [20]. As a promoter, the neuron-specific synapsin I promoter was selected. Human GLUT1 shares high homology with mouse GLUT1 (96% identical at the amino acid level; assessed by NCBI BLAST). To establish a therapeutic strategy, we compared systemic and local administration mouse models of GLUT1DS. For systemic/local administration, we selected intraperitoneal/intra-cerebroventricular injection, respectively.

3.2. GLUT1 protein expression after infection with AAV-hSLC2A1 in cultured cells

Before injection to mice, we confirmed exogenous GLUT1 protein expression in SH-SY5Y cells. After infection with AAV-h*SLC2A1*, the cells were stained using an anti-myc antibody. Exogenous GLUT1 was expressed in the cell body, especially at the peri-membranous region (Fig. 2a; arrow). The cellular localization of anti-myc immunoreactivity was similar to that of an anti-GLUT1 antibody and they both overlapped when their respective images were merged (Fig. 2b).

3.3. Expression of GLUT1 after the administration of AAV-hSLC2A1 to GLUT1$^{+/-}$ mice

Local or systemic administration of AAV-h*SLC2A1* to GLUT1$^{+/-}$ mice was performed. We assessed the mRNA and protein expression of GLUT1. Vector-derived RNA was detected in both the intra-cerebroventricular and intraperitoneal injection groups (Fig. 3a, b). In quantitative PCR of *GLUT1-myc*, exogenous *GLUT1* (*GLUT1-myc*) was detected in both injection groups, but not in the control group (Fig. 3b). The total amount of *GLUT1* mRNA was increased 2.4-fold in the intra-cerebroventricular injection group ($n = 3$, $P < 0.05$) and 1.6-fold in the intraperitoneal injection group compared to the control GLUT1$^{+/-}$ group (Fig. 3c).

Exogenous GLUT1 protein (GLUT1-myc protein) was identified in brain tissue by immunofluorescence analysis. We first examined intrinsic GLUT1 expression using GLUT1$^{+/-}$ mice. As reported previously, the anti-GLUT1 antibody stained neurons, oligodendrocytes, astrocytes, and endothelial cells (Supplementary Fig. 1). At 3 months after intra-cerebroventricular injection, GLUT1-myc was strongly detected at the periventricular cerebral cortex and hippocampus nearby the injection site (Fig. 4d, e, f); however, it was not detected in distantly positioned brain areas (Fig. 4c). Exogenous GLUT1 was expressed mainly in neural cells. Moreover, myc-immunoreactivity was observed in oligodendrocytes (anti-myelin proteolipid protein) and endothelial cells (anti-CD31) (Fig. 5). Reflecting exogenous GLUT1 protein expression, total GLUT1 protein from both intrinsic and exogenous GLUT1 was strongly expressed in cortical and hippocampal neurons (Supplementary Fig. 2a, c).

At 3 months after intraperitoneal injection, a modest level of GLUT1-myc was detected in the cerebral cortex and hippocampus (Fig. 6c, d, e), and cerebellum (Fig. 6f).

We also assessed GLUT1 mRNA and protein expression after intra-cerebroventricular injection with untagged AAV-h*SLC2A1*. The total amount of *GLUT1* mRNA also increased in the untagged AAV-h*SLC2A1* injection group compared to the control GLUT1$^{+/-}$ group (Supplementary Fig. 3). In the untagged AAV-h*SLC2A1* injection group, GLUT1 protein was strongly expressed in the cortex and hippocampus nearby the injection site (Supplementary Fig. 4), but the total amount of GLUT1 protein in the whole cerebrum was not significantly different ($P = 0.81$, Supplementary Fig. 5). At the age of 14 weeks, the average body weight of GLUT1$^{+/+}$ mice was 22.2 ± 1.5 g ($n = 9$), and the average body weight of GLUT1$^{+/-}$ mice was not significantly different with 19.6 ± 1.0 g ($n = 6$). After intra-cerebroventricular injection, the average body weight of AAV-treated GLUT1$^{+/-}$ mice at the age of 14 weeks, corresponding to 8 weeks after intra-cerebroventricular injection, was 21.2 ± 2.0 g ($n = 6$) (Supplementary Fig. 6a). At the age of 14 weeks, the average cerebral hemisphere weight of GLUT1$^{+/+}$ mice (213.3 ± 8.8 mg, $n = 3$) and GLUT1$^{+/-}$ mice (136.6 ± 6.6 mg, $n = 6$) were significantly different ($P < 0.05$), as reported previously [19]. After

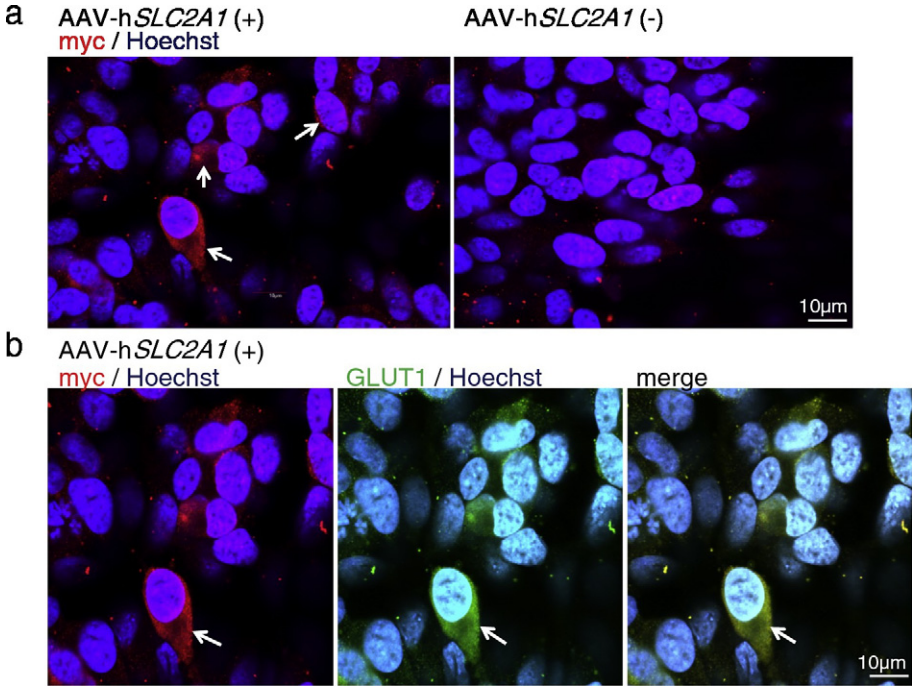

Fig. 2. GLUT1-myc expression in SH-SY5Y cells after infection with AAV-h*SLC2A1*. (a) Exogenous GLUT1 expression, confirmed using an anti-myc antibody. Exogenous GLUT1 was immunostained with an anti-myc antibody. GLUT1 was expressed in the cell body, especially at the peri-membranous region (arrow). (b) Whole GLUT1 expression confirmed using an anti-GLUT1 antibody. The intra-cellular localization of myc-immunoreactivity was similar to that of an anti-GLUT1 antibody (arrow). Both anti-myc and anti-GLUT1 immunoreactivities overlapped in the merge image.

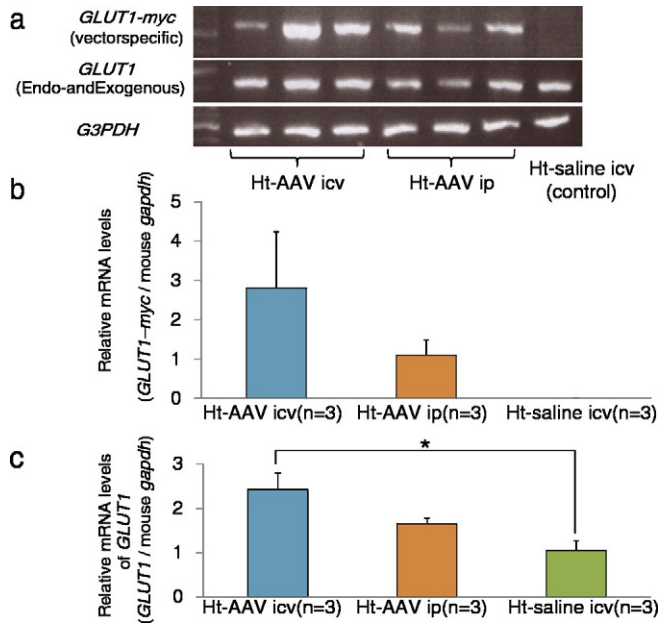

Fig. 3. *GLUT1* mRNA expression in the whole cerebrum after injection with AAV-h*SLC2A1*. At 2 months after intraperitoneal or intra-cerebroventricular injection, total RNA was extracted from whole cerebrum. As a control, GLUT1$^{+/-}$ mice were injected with saline into the bilateral lateral ventricles at the age of 6 weeks. Total RNA from the whole cerebrum of the control GLUT1$^{+/-}$ group was extracted in the same way. Ht: GLUT1$^{+/-}$ mouse; icv: intra-cerebroventricular injection; ip: intraperitoneal injection. (a) Vector-specific RT-PCR. Vector-derived RNA was assessed using primer sets containing a myc-tag-specific sequence. Vector-derived RNA was detected in both injection groups. (b) Quantitative PCR of *GLUT1-myc*. mRNA expression of exogenous *GLUT1* was detected using primers contained a myc-tag-specific sequence. The relative mRNA levels of *GLUT1-myc* were higher in the intra-cerebroventricular injection group than in the intraperitoneal injection group. *GLUT1-myc* mRNA was not detected in the control GLUT1$^{+/-}$ group. (c) Quantitative PCR of *GLUT1*. The total amount of *GLUT1* mRNA was measured using primers corresponding to human and murine *SLC2A1* sequences. The bar graph indicates the relative levels of *GLUT1* mRNA to GLUT1$^{+/-}$ mice without injection. The total amount of *GLUT1* mRNA was increased 2.4-fold in the intra-cerebroventricular injection group ($P < 0.05$) and 1.6-fold in the intraperitoneal injection group relative to the control GLUT1$^{+/-}$ group. *$P < 0.05$. Bar height; mean ± standard error (SE).

intra-cerebroventricular injection, the cerebral hemisphere weight of AAV-treated GLUT1$^{+/-}$ mice at the age of 14 weeks approached to wild type with no significant difference to wild type or no-injected heterozygous (160 ± 20.4 mg; n = 6) (Supplementary Fig. 6b).

3.4. Improvement of motor function and CSF glucose levels after the administration of AAV-hSLC2A1 to GLUT1$^{+/-}$ mice

We assessed motor function after injection using rota-rod and footprint tests. Fig. 7 shows the results of the rota-rod test at the age of 10 and 14 weeks, corresponding to 4 and 8 weeks after intra-cerebroventricular injection, respectively. In our study, the rota-rod test at the age of 6 weeks of GLUT1$^{+/+}$ mice and untreated GL UT1$^{+/-}$ mice was not significantly different (207.5 ± 14.0 s (n = 16) vs. 182.4 ± 11.0 s (n = 22), P = 0.16; data not shown). Rota-rod test of control GLUT1$^{+/-}$ mice (GLUT1$^{+/-}$ mice after intra-cerebroventricular injection with saline) (Fig. 7) showed significantly shorter time than that of wild, GLUT1$^{+/+}$ mice at 10 and 14 weeks (Fig. 7, $P < 0.05$). There was no significant deference between untreated GLUT1$^{+/-}$ mice and saline-injected GLUT1$^{+/-}$ mice (data not shown). In both injection groups, the rota-rod test showed trends for motor function improvement compared with the control GLUT1$^{+/-}$ group at both 10 and 14 weeks (Fig. 7). Especially, at 4 weeks after intra-cerebroventricular injection of the untagged AAV-h*SLC2A1* group, motor function was significantly improved to the level of wild-type mice ($n = 7$, $P < 0.05$). The footprint test showed no statistical difference between the injected GLUT1$^{+/-}$ mice and control GLUT1$^{+/-}$ mice (data not shown). For biochemical analysis, we measured CSF and blood glucose levels in samples collected from GLUT1$^{+/-}$ mice at 8 weeks after intra-cerebroventricular injection with AAV-h*SLC2A1*. The CSF glucose level was significantly higher in GLUT1$^{+/+}$ mice (92.4 ± 7.9 mg/dl, n = 9) than in GLUT1$^{+/-}$ mice (66 ± 3.8 mg/dl, n = 9) ($P < 0.05$), and the CSF/blood glucose ratio was significantly higher in GLUT1$^{+/+}$ mice (0.69 ± 0.05, n = 7) than in GLUT1$^{+/-}$ mice (0.42 ± 0.01, n = 6) as reported previously [19]. The CSF glucose levels were partially restored after injection compared to GLUT1$^{+/-}$ mice without treatment (87.5 ± 12.1 mg/dL vs. 71.3 ± 4.3 mg/dL,

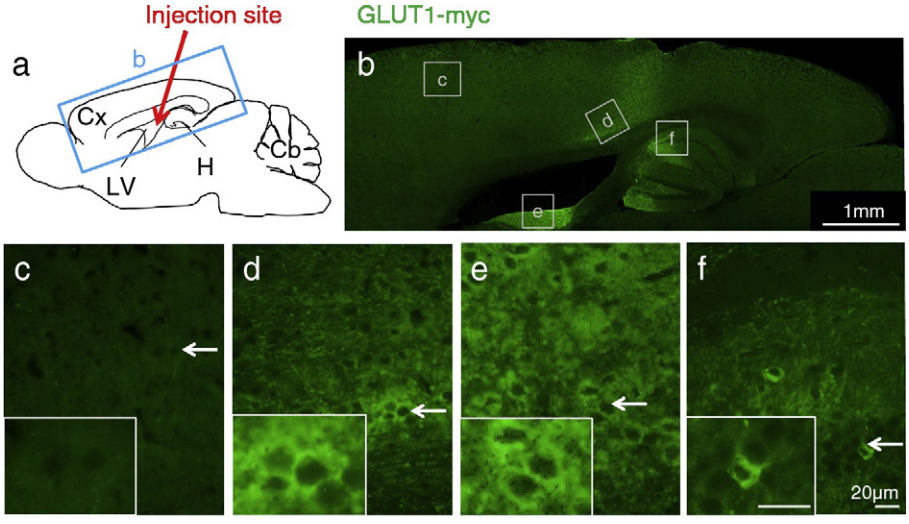

Fig. 4. Immunofluorescence of mouse brain after intra-cerebroventricular injection with AAV-h*SLC2A1*. At 3 months after AAV-hSLC2A1 injection, exogenous GLUT1 (GLUT1-myc) protein was detected using an anti-myc primary antibody and an anti-rabbit IgG Alexa Fluor 488 secondary antibody. (a) Schematic diagram of a sagittal section of mouse brain. The red arrow indicates the injection site. Cx: cerebral cortex; LV: lateral ventricle; H: hippocampus; Cb: cerebellum. (b–f) Immunofluorescence of sagittal sections of the whole cerebrum. Whole brain sagittal sections showing the gradient of expression. The area around the injected site was strongly stained with an anti-myc antibody (a). A high level of exogenous GLUT1 was detected in the cerebral cortex and hippocampus nearby the injection site (d, e, f), but exogenous GLUT1 was not detected at areas distant from the injection site (c). The midbrain, pons, cerebellum, and medulla were not stained by the anti-myc antibody. Inset image indicates typical cells (c, d, e, f; arrow) stained by the anti-myc antibody. The scale bar in the inset image indicates 20 μm.

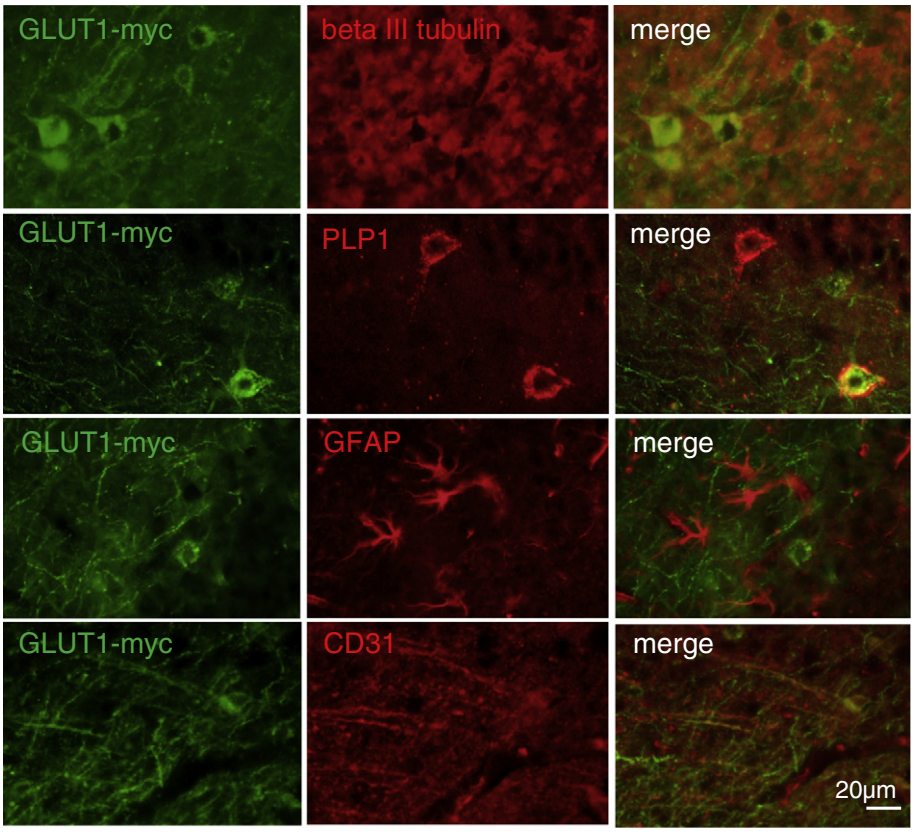

Fig. 5. Types of cells in brain tissue that were stained by an anti-myc antibody. Exogenous GLUT1 (GLUT1-myc) expression was detected with an anti-myc primary antibody and an anti-rabbit IgG Alexa Fluor 488 secondary antibody. Myc-immunoreactive cells were co-stained using anti-beta III tubulin (neuron-specific marker), anti-PLP1 (oligodendrocyte marker), anti-GFAP (astrocyte marker), and anti-CD31 (endothelial marker) primary antibodies, and anti-goat IgG Alexa Fluor 594 and anti-chicken IgY Alexa Fluor 594 secondary antibodies. Myc-immunoreactive cells were co-stained by the anti-beta III tubulin antibody, but not stained by the anti-GFAP antibody. Some of the myc-immunoreactive cells were stained by the anti-PLP1 and CD31 antibodies.

respectively), and the CSF/blood glucose ratio was significantly elevated after injection compared to GLUT1$^{+/-}$ mice without treatment (0.495 vs. 0.42, respectively, $P < 0.05$; diagnostic criterion for GLUT1DS was <0.45) (Fig. 8).

4. Discussion

Previously, by using an enzymatic photometric 2-deoxyglucose uptake assay, we reported that the degree of glucose uptake impairment

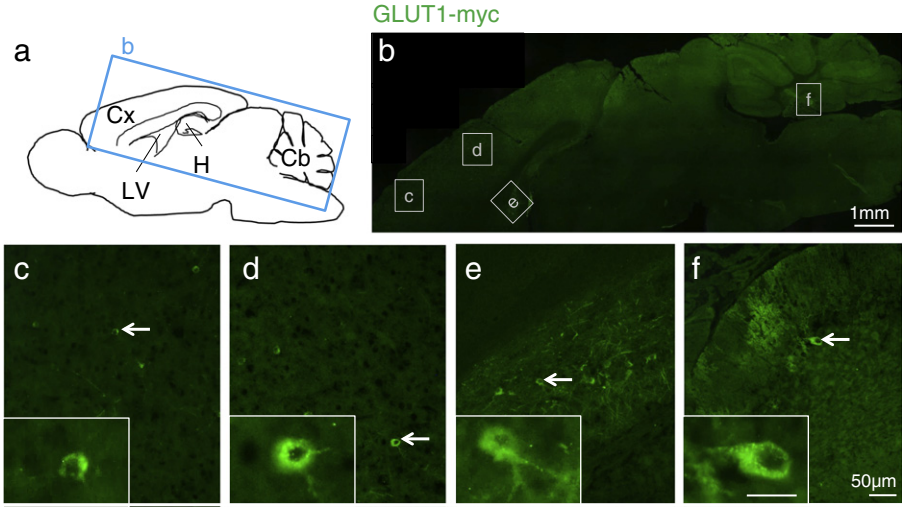

Fig. 6. Immunofluorescence of mouse brain after intraperitoneal injection with AAV-h*SLC2A1*. At 3 months after AAV9-h*SLC2A1* injection, exogenous GLUT1 (GLUT1-myc) expression was detected with anti-myc and anti-rabbit IgG Alexa Fluor 488 antibodies in the same manner as for intra-cerebroventricular injection (Fig. 4). (a) Schematic diagram of a sagittal section of mouse brain. Cx: cerebral cortex; LV: lateral ventricle; H: hippocampus; Cb: cerebellum. (b) Sagittal section of the whole cerebrum under low magnification. (c–f) Immunofluorescence of cerebral cortex, hippocampus, and cerebellar sections using an anti-myc antibody. Modest levels of GLUT1-myc were detected in the cerebral cortex (c, d), hippocampus (e), and midbrain. GLUT1-myc was also detected in cerebellar Purkinje cells (f). Inset image indicates typical cells (c, d, e, f; arrow) stained by the anti-myc antibody. The scale bar in the inset image indicates 20 μm.

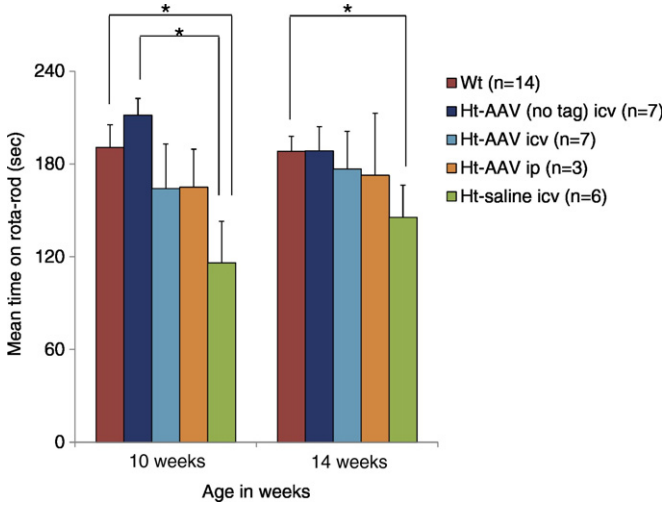

Fig. 7. Rota-rod test after AAV-h*SLC2A1* injection. The mice were trained in acceleration mode from 4 to 40 rpm 3 times daily for 2 continuous days. At 30 min after the final training session on the second day, the mice were tested. The bar graph shows the time taken to fall off the rotating drum during the final test. The rota-rod test was performed at the age of 10 and 14 weeks, corresponding to 4 and 8 weeks after intra-cerebroventricular injection, respectively. There was a significant deference between Wt ($GLUT1^{+/+}$) mice and control $GLUT1^{+/-}$ mice ($GLUT1^{+/-}$ mice after intra-cerebroventricular injection with saline) ($P < 0.05$). In both injection groups, the Rota-rod test showed trends for motor function improvement compared with control $GLUT1^{+/-}$ mice. Especially, at 4 weeks after intra-cerebroventricular injection of the untagged AAV-h*SLC2A1* group, motor function was significantly improved ($P < 0.05$). *$P < 0.05$. Bar height; mean ± SE. Wt: $GLUT1^{+/+}$ mice; Ht: $GLUT1^{+/-}$ mice; icv: intra-cerebroventricular injection; ip: intraperitoneal injection; Ht-AAV (no tag) icv: $GLUT1^{+/-}$ mice after intra-cerebroventricular injection of untagged AAV-h*SLC2A1*.

by *SLC2A1* determines disease severity in GLUT1DS patients [22]. As the loss of glucose transport ability was correlated with disease severity, we aimed to deliver *SLC2A1* as gene therapy for GLUT1DS. Here, we confirmed the expression of *SLC2A1* in neuronal cells of $GLUT1^{+/-}$ mice after injection of AAV-h*SLC2A1*, which expresses the human *SLC2A1* gene under the control of the synapsin I promoter. Motor function analysis using the rota-rod test showed trends for motor function improvement after intraperitoneal and intra-cerebroventricular injection. Especially, motor function was significantly improved after intra-cerebroventricular injection of AAV-h*SLC2A1*.

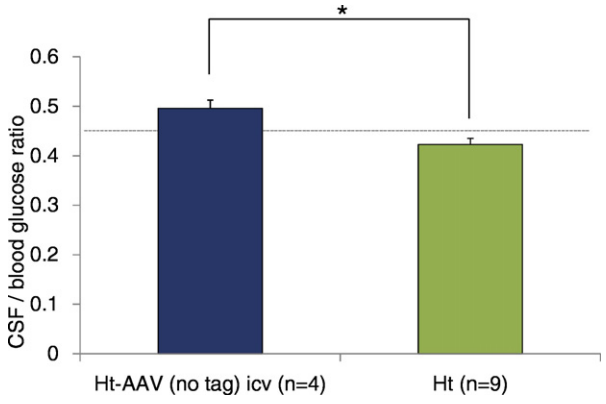

Fig. 8. CSF/blood glucose ratio after AAV9-h*SLC2A1* injection. CSF and blood glucose collected from Ht ($GLUT1^{+/-}$; $n = 6$) and $GLUT1^{+/-}$ mice after intra-cerebroventricular injection with untagged AAV9-h*SLC2A1* ($n = 4$). Bar graph shows the CSF/blood glucose ratio, and the diagnostic criterion for GLUT1DS is indicated by the dotted line (<0.45). The CSF/blood glucose ratio in $GLUT1^{+/-}$ mice after intra-cerebroventricular injection with untagged AAV9-h*SLC2A1* (0.495 ± 0.01, $n = 4$) was significantly improved compared to $GLUT1^{+/-}$ mice (0.42 ± 0.01, $n = 6$), >0.45 ($P < 0.05$). *$P < 0.05$. Bar height; mean ± SE. Ht-AAV (no tag) icv: $GLUT1^{+/-}$ mice after intra-cerebroventricular injection of untagged AAV-h*SLC2A1*.

4.1. Selection of the AAV vector with the synapsin I promoter for GLUT1DS treatment

We selected the tyrosine-mutant AAV9/3 vector for gene therapy of GLUT1DS. Intravenously injected AAV9-based vectors at neonatal period reportedly pass through the blood-brain barrier and transduce widespread neuronal targets including the striatum, cortex, anterior commissure, internal capsule, corpus callosum, hippocampus, dentate gyrus, midbrain, and cerebellum [23]. Moreover, the tyrosine-mutant AAV9/3 vector was able to induce widespread transgene expression in the brain and spinal cord of adult mice [20]. As patients with GLUT1DS were diagnosed at Childhood, and impaired hexose transport throughout the brain, we selected tyrosine-mutant AAV9/3 as a suitable vector for gene therapy of GLUT1DS.

We selected the synapsin I promoter to drive expression in our curative AAV vector as it has already been used successfully in several mouse models [20,24,25]. The synapsin I promoter activates expression mainly in neural cells and has a reduced off-target effect when delivered systemically. In the CNS, GLUT1, GLUT3, and monocarboxylate transporter 1/2/3/4 have major roles in the glucose and lactate transport metabolic pathway [5,18,26]. However, heterozygous knockout of GLUT3 did not impair glucose uptake in a mouse model [27]. We confirmed intrinsic GLUT1 protein expression in endothelial cells, astrocytes, oligodendrocytes, and neural cells (Supplementary Fig. 1), and exogenous GLUT1 expression under the control of the synapsin I promoter was mainly detected in neural cells and to a lesser extent in oligodendrocytes and endothelial cells. It may be possible that glucose levels and motor performance could be improved further if GLUT1 can be expressed in a more similar manner as the intrinsic expression pattern among different cell types in the CNS. Therefore, we are now investigating a minimal endogenous promoter that approximates human physiological GLUT1 expression within the range of the limited length of the AAV insert.

4.2. Selection of optimal injection route

In our immunohistochemistry results, weak expression of exogenous GLUT1 was detected throughout the brain, including the cerebellum, after intraperitoneal injection. Strong expression of exogenous GLUT1 was detected nearby the injection site of brain tissue after intra-cerebroventricular injection.

In previous reports, in which different injection routes of AAV9 were compared, direct cerebellar cortex injection (DC injection) resulted in robust expression limited to the cerebellum. Intrathecal space injection into the cisterna magna resulted in a more broad area of expression than DC injection, including the cerebrum, brainstem, spinal cord, and a limited part of the cerebellum nearby the injection site. Intravenous injection resulted in very weak expression spanning the entire CNS [28–30]. Systemic administration appears to be advantageous for the expression of GLUT1 throughout the brain, but it needs the delivery of a large amount of AAV vector. Injection of AAV-h*SLC2A1* to neonatal or fetal mouse may be improved its transduction efficiency to the CNS because it is easier for AAV to pass through the blood-brain barrier. In addition, this could prevent brain damage before clinical manifestation.

In our study, intra-cerebroventricular injection produced stronger GLUT1 expression with ~1/10 of the dose of AAV-h*SLC2A1* vector required for intraperitoneal injection. Moreover, intra-cerebroventricular injection produced a significant increase of glucose in the CSF and motor improvement, even with restricted expression. Injection to the cisterna magna, or a less invasive intrathecal injection, appears a plausible route for gene therapy in humans. We did not perfume the dose response study here. In addition to the route, optimizing the dose would bear better yield of expression.

In conclusion, we showed both intraperitoneal and cerebroventricular injected AAV-h*SLC2A1* expressed exogenous GLUT1 mRNA and protein in brain tissues, and improved motor function and CSF glucose levels in *Glut1*-deficient mice. After choosing best promoter,

injection route, and optimal dosing, gene therapy using an AAV vector would be a promising approach for the treatment of GLUT1DS.

Conflict of interest statement

S. M. owns equity in a gene therapy company (Gene Therapy Research Institution) that commercializes the use of AAV vectors for gene therapy applications. To the extent that the work in this manuscript increases the value of these commercial holdings, S. M. has a conflict of interest.

Acknowledgements

This work was supported by grants from the Japan Society for the Promotion of Science, JSPS KAKENHI and grants for the Project for Health Research on Infants, Children, Adolescents, and Young Adults from Japan Agency for Medical Research and Development.

Appendix A. Supplementary data

Supplementary data to this article can be found online at http://dx.doi.org/10.1016/j.ymgmr.2016.12.008.

References

[1] F. Maher, S.J. Vannucci, I.A. Simpson, Glucose transporter proteins in brain, FASEB J. 8 (1994) 1003–1011.
[2] S.J. Vannucci, F. Maher, I.A. Simpson, Glucose transporter proteins in brain: delivery of glucose to neurons and glia, Glia 21 (1997) 2–21.
[3] I.A. Simpson, A. Carruthers, S.J. Vannucci, Supply and demand in cerebral energy metabolism: the role of nutrient transporters, J. Cereb. Blood Flow Metab. 27 (2007) 1766–1791.
[4] C. Choeiri, W. Staines, C. Messier, Immunohistochemical localization and quantification of glucose transporters in the mouse brain, Neuroscience 111 (2002) 19–34.
[5] M.S. Hildebrand, J.A. Damiano, S.A. Mullen, S.T. Bellows, K.L. Oliver, H.H. Dahl, I.E. Scheffer, S.F. Berkovic, Glucose metabolism transporters and epilepsy: only GLUT1 has an established role, Epilepsia 55 (2014) e18–e21.
[6] J. Klepper, B. Leiendecker, GLUT1 deficiency syndrome—2007 update, Dev. Med. Child Neurol. 49 (2007) 707–716.
[7] V. De Giorgis, P. Veggiotti, GLUT1 deficiency syndrome 2013: current state of the art, Seizure 22 (2013) 803–811.
[8] Y. Ito, S. Takahashi, K. Kagitani-Shimono, J. Natsume, K. Yanagihara, T. Fujii, H. Oguni, Nationwide survey of glucose transporter-1 deficiency syndrome (GLUT-1DS) in Japan, Brain Dev. 37 (2015) 780–789.
[9] W.G. Leen, R.A. Wevers, E.J. Kamsteeg, H. Scheffer, M.M. Verbeek, M.A. Willemsen, Cerebrospinal fluid analysis in the workup of GLUT1 deficiency syndrome: a systematic review, JAMA. Neurol. 70 (2013) 1440–1444.
[10] W.G. Leen, M. Taher, M.M. Verbeek, E.J. Kamsteeg, B.P. van de Warrenburg, M.A. Willemsen, GLUT1 deficiency syndrome into adulthood: a follow-up study, J. Neurol. 261 (2014) 589–599.
[11] J. Klepper, Glucose transporter deficiency syndrome (GLUT1DS) and the ketogenic diet, Epilepsia 49 (Suppl. 8) (2008) 46–49.
[12] T. Fujii, Y. Ito, S. Takahashi, K. Shimono, J. Natsume, K. Yanagihara, H. Oguni, Outcome of ketogenic diets in GLUT1 deficiency syndrome in Japan: a nationwide survey, Brain Dev. 38 (2016) 628–637.
[13] Y. Ito, H. Oguni, S. Ito, M. Oguni, M. Osawa, A modified Atkins diet is promising as a treatment for glucose transporter type 1 deficiency syndrome, Dev. Med. Child Neurol. 53 (2011) 658–663.
[14] P.O. Kwiterovich Jr., E.P. Vining, P. Pyzik, R. Skolasky Jr., J.M. Freeman, Effect of a high-fat ketogenic diet on plasma levels of lipids, lipoproteins, and apolipoproteins in children, JAMA 290 (2003) 912–920.
[15] F. Mochel, E. Hainque, D. Gras, I.M. Adanyeguh, S. Caillet, B. Heron, A. Roubertie, E. Kaphan, R. Valabregue, D. Rinaldi, S. Vuillaumier, R. Schiffmann, C. Ottolenghi, J.Y. Hogrel, L. Servais, E. Roze, Triheptanoin dramatically reduces paroxysmal motor disorder in patients with GLUT1 deficiency, J. Neurol. Neurosurg. Psychiatry 87 (2016) 550–553.
[16] W.L. Hwu, S. Muramatsu, S.H. Tseng, K.Y. Tzen, N.C. Lee, Y.H. Chien, R.O. Snyder, B.J. Byrne, C.H. Tai, R.M. Wu, Gene therapy for aromatic L-amino acid decarboxylase deficiency, Sci. Transl. Med. 4 (2012) 134ra161.
[17] H. Fu, M.P. Cataldi, T.A. Ware, K. Zaraspe, A.S. Meadows, D.A. Murrey, D.M. McCarty, Functional correction of neurological and somatic disorders at later stages of disease in MPS IIIA mice by systemic scAAV9-hSGSH gene delivery, Mol. Ther. Methods Clin. Dev. 3 (2016) 16036.
[18] S. Ohtsuki, T. Kikkawa, S. Hori, T. Terasaki, Modulation and compensation of the mRNA expression of energy related transporters in the brain of glucose transporter 1-deficient mice, Biol. Pharm. Bull. 29 (2006) 1587–1591.
[19] D. Wang, J.M. Pascual, H. Yang, K. Engelstad, X. Mao, J. Cheng, J. Yoo, J.L. Noebels, D.C. De Vivo, A mouse model for Glut-1 haploinsufficiency, Hum. Mol. Genet. 15 (2006) 1169–1179.
[20] A. Iida, N. Takino, H. Miyauchi, K. Shimazaki, S. Muramatsu, Systemic delivery of tyrosine-mutant AAV vectors results in robust transduction of neurons in adult mice, Biomed. Res. Int. 2013 (2013) 974819.
[21] R.B. DeMattos, K.R. Bales, M. Parsadanian, M.A. O'Dell, E.M. Foss, S.M. Paul, D.M. Holtzman, Plaque-associated disruption of CSF and plasma amyloid-beta (Abeta) equilibrium in a mouse model of Alzheimer's disease, J. Neurochem. 81 (2002) 229–236.
[22] S. Nakamura, H. Osaka, S. Muramatsu, S. Aoki, E.F. Jimbo, T. Yamagata, Mutational and functional analysis of glucose transporter I deficiency syndrome, Mol. Genet. Metab. 116 (2015) 157–162.
[23] K.D. Foust, E. Nurre, C.L. Montgomery, A. Hernandez, C.M. Chan, B.K. Kaspar, Intravascular AAV9 preferentially targets neonatal neurons and adult astrocytes, Nat. Biotechnol. 27 (2009) 59–65.
[24] N. Iwata, M. Sekiguchi, Y. Hattori, A. Takahashi, M. Asai, B. Ji, M. Higuchi, M. Staufenbiel, S. Muramatsu, T.C. Saido, Global brain delivery of neprilysin gene by intravascular administration of AAV vector in mice, Sci. Rep. 3 (2013) 1472.
[25] T. Yamashita, H.L. Chai, S. Teramoto, S. Tsuji, K. Shimazaki, S. Muramatsu, S. Kwak, Rescue of amyotrophic lateral sclerosis phenotype in a mouse model by intravenous AAV9-ADAR2 delivery to motor neurons, EMBO. Mol. Med. 5 (2013) 1710–1719.
[26] L.B. Gladden, Lactate metabolism: a new paradigm for the third millennium, J. Physiol. 558 (2004) 5–30.
[27] C.A. Stuart, I.R. Ross, M.E. Howell, M.P. McCurry, T.G. Wood, J.D. Ceci, S.J. Kennel, J. Wall, Brain glucose transporter (Glut3) haploinsufficiency does not impair mouse brain glucose uptake, Brain Res. 1384 (2011) 15–22.
[28] L. Samaranch, E.A. Salegio, W. San Sebastian, A.P. Kells, K.D. Foust, J.R. Bringas, C. Lamarre, J. Forsayeth, B.K. Kaspar, K.S. Bankiewicz, Adeno-associated virus serotype 9 transduction in the central nervous system of nonhuman primates, Hum. Gene Ther. 23 (2012) 382–389.
[29] L. Samaranch, E.A. Salegio, W. San Sebastian, A.P. Kells, J.R. Bringas, J. Forsayeth, K.S. Bankiewicz, Strong cortical and spinal cord transduction after AAV7 and AAV9 delivery into the cerebrospinal fluid of nonhuman primates, Hum. Gene Ther. 24 (2013) 526–532.
[30] F. Huda, A. Konno, Y. Matsuzaki, H. Goenawan, K. Miyake, T. Shimada, H. Hirai, Distinct transduction profiles in the CNS via three injection routes of AAV9 and the application to generation of a neurodegenerative mouse model, Mol. Ther. Methods Clin. Dev. 1 (2014) 14032.